Redox Biology 37 (2020) 101740

Contents lists available at ScienceDirect

Redox Biology

journal homepage: www.elsevier.com/locate/redox

SOD2 deficiency in cardiomyocytes defines defective mitochondrial bioenergetics as a cause of lethal dilated cardiomyopathy

Sudha Sharma [a], Susmita Bhattarai [a], Hosne Ara [a], Grace Sun [a], Daret K. St Clair [b], Md Shenuarin Bhuiyan [c], Christopher Kevil [c], Megan N. Watts [d], Paari Dominic [d], Takahiko Shimizu [e], Kevin J. McCarthy [a], Hong Sun [a], Manikandan Panchatcharam [a,**], Sumitra Miriyala [a,*]

[a] Department of Cellular Biology and Anatomy, Louisiana State University Health Sciences Center, Shreveport, LA, USA
[b] Department of Toxicology and Cancer Biology, College of Medicine, University of Kentucky, Lexington, KY, USA
[c] Department of Pathology and Translational Pathobiology, Louisiana State University Health Sciences Center, Shreveport, LA, USA
[d] Division of Cardiology, Department of Medicine, Louisiana State University Health Sciences Center, Shreveport, LA, USA
[e] National Center for Geriatrics and Gerontology, 7-430, Morioka, Obu Aichi, Japan

ARTICLE INFO

Keywords:
Heart failure
Manganese superoxide dismutase
Superoxide radicals

ABSTRACT

Electrophilic aldehyde (4-hydroxynonenal; 4-HNE), formed after lipid peroxidation, is a mediator of mitochondrial dysfunction and implicated in both the pathogenesis and the progression of cardiovascular disease. Manganese superoxide dismutase (MnSOD), a nuclear-encoded antioxidant enzyme, catalyzes the dismutation of superoxide radicals ($O_2^{\bullet-}$) in mitochondria. To study the role of MnSOD in the myocardium, we generated a cardiomyocyte-specific *SOD2* (*SOD2Δ*) deficient mouse strain. Unlike global *SOD2* knockout mice, *SOD2Δ* mice reached adolescence; however, they die at ~4 months of age due to heart failure. Ultrastructural analysis of *SOD2Δ* hearts revealed altered mitochondrial architecture, with prominent disruption of the cristae and vacuole formation. Noninvasive echocardiographic measurements in $SOD2^{\Delta}$ mice showed dilated cardiomyopathic features such as decreased ejection fraction and fractional shortening along with increased left ventricular internal diameter. An increased incidence of ventricular tachycardia was observed during electrophysiological studies of the heart in *SOD2Δ* mice. Oxidative phosphorylation (OXPHOS) measurement using a Seahorse XF analyzer in *SOD2Δ* neonatal cardiomyocytes and adult cardiac mitochondria displayed reduced O_2 consumption, particularly during basal conditions and after the addition of FCCP (H^+ ionophore/uncoupler), compared to that in *SOD2fl* hearts. Measurement of extracellular acidification (ECAR) to examine glycolysis in these cells showed a pattern precisely opposite that of the oxygen consumption rate (OCR) among *SOD2Δ* mice compared to their $SOD2^{fl}$ littermates. Analysis of the activity of the electron transport chain complex identified a reduction in Complex I and Complex V activity in *SOD2Δ* compared to *SOD2fl* mice. We demonstrated that a deficiency of SOD2 increases reactive oxygen species (ROS), leading to subsequent overproduction of 4-HNE inside mitochondria. Mechanistically, proteins in the mitochondrial respiratory chain complex and TCA cycle (NDUFS2, SDHA, ATP5B, and DLD) were the target of 4-HNE adduction in *SOD2Δ* hearts. Our findings suggest that the SOD2 mediated 4-HNE signaling nexus may play an important role in cardiomyopathy.

1. Introduction

Dilated cardiomyopathy (DCM), a significant risk factor for heart failure, is characterized by enlargement of the left ventricle with impaired systolic function in the absence of underlying systemic conditions such as hypertension, valvular heart disease, or coronary artery disease [1]. Both genetic and non-genetic factors are associated with this disease, and evidence suggests that various proteins located in the mitochondria responsible for energy metabolism and other functions are involved in its initiation and progression [2]. Recently, a *SOD2*

* Corresponding author. Department of Cellular Biology and Anatomy, LSUHSC-Shreveport, PO Box 33932, Shreveport, LA, 71130-3932, USA.
** Corresponding author. Department of Cellular Biology and Anatomy, LSUHSC-Shreveport, PO Box 33932, Shreveport, LA, 71130-3932, USA..
E-mail addresses: mpanch@lsuhsc.edu (M. Panchatcharam), smiriy@lsuhsc.edu (S. Miriyala).

https://doi.org/10.1016/j.redox.2020.101740
Received 16 July 2020; Received in revised form 1 September 2020; Accepted 23 September 2020
Available online 30 September 2020

homozygous variant was identified as a causative factor for lethal dilated cardiomyopathy in humans where the homozygous missense variant, c.542 g > t, p. (gly181Val), was observed in the *SOD2* gene. This points to the potential role played by oxidative stress in the etiology and pathogenesis of dilated cardiomyopathy [3].

Mitochondria perform several roles to maintain cellular function. They are producers of ATP, involved in cellular Ca^{2+} homeostasis, and mediate apoptosis. The electron transport chain, comprising five multiprotein complexes (I–V), is embedded in the inner mitochondrial membrane, and a series of electron transfers and H^{+} translocation occurs via the actions of these complexes to generate ATP. In addition, mitochondria are a major contributor to the generation of reactive oxygen species (ROS) via the respiratory complex under physiological conditions [4,5]. Mitochondrial abnormalities related to ROS production, mitochondrial bioenergetics, mitochondrial dynamics, and the mitochondrial ability to buffer ions have been linked to heart failure. Given that mitochondrial bioenergetics and ROS are closely related, it is imperative to address these aspects of mitochondrial dysfunction together to understand the mechanism of heart failure [6]. The inner mitochondrial membrane is made up of a unique phospholipid called cardiolipin; mammalian cardiolipin occurs in the form of the dimer tetralinoleoyl CL (L4CL). Owing to the polyunsaturated fatty acid nature of L4CL and its proximity to the mitochondrial respiratory complex, it is highly susceptible to lipid peroxidation, which leads to the formation of a reactive aldehyde known as 4-hydroxynoneal (4-HNE) [7]. Depending upon the concentration, 4-HNE can be detrimental or beneficial to the cell; however, at pathological concentrations, it can cause cellular death [8].

Manganese superoxide dismutase (*SOD2* or MnSOD), a mitochondrial matrix-based antioxidant enzyme, is responsible for scavenging locally produced free radicals. It converts these free radicals into hydrogen peroxide and then into water with the help of catalase, peroxiredoxins (Prxs), or glutathione peroxidases (GPx), for survival [9]. Global knockout mice devoid of *SOD2* died around 10 days after birth due to complications from dilated cardiomyopathy, metabolic acidosis, and lipid deposition in skeletal muscle and liver [10]. Given the short life span of global knockout mice, we generated conditional cardiomyocyte-specific knockout mice to help us better understand the underlying pathogenesis of heart failure.

In this study, we found that cardiomyocyte-specific *SOD2* knockout causes a characteristic feature in mice, dilated cardiomyopathy, and subsequent death due to heart failure. We also observed that *SOD2* deficiency in cardiomyocytes leads to the overproduction of intramitochondrial 4-HNE. This overabundant 4-HNE binds to the proteins of the mitochondrial respiratory complex and TCA cycle, thereby causing decreased mitochondrial respiration.

2. Material and methods

2.1. Cardiac-specific deletion of SOD2 in mice

All the animal handling protocols were approved by the IACUC, Louisiana State University Health Sciences Center-Shreveport, and performed in accordance with the National Institutes of Health Guide for the Care and Use of Laboratory Animals. The production and initial characterization of mice carrying a conditional allele of *SOD2* (*SOD2fl*) was performed as described previously [11]. Ten generations of *SOD2*fl mice were back-crossed with C57Bl/6 mice to ensure a stable genotype. *SOD2fl* mice were crossed with C57Bl/6 mice expressing Cre recombinase controlled under a cardiac-specific alpha-myosin heavy chain promoter (*Myh6-Cre*) [12] to generate cardiac-specific *SOD2Δ* mice. Mating of homozygous *SOD2fl* with *SOD2Δ* mice yielded 50% *SOD2Δ* offspring with less than 2% mortality at birth. The mice were fed Purina 5058 rodent chow and water ad libitum and housed in HEPA-filtered air rooms with 12-h light/dark cycles. Mouse genotyping was carried out using DNA samples obtained from tail snips and the PCR primers P1=CGAGGGGCATCTAGTGGAGAAG, P2 = TTAGGGCTCAGGTTTGT CCAGAA, and P4 = AGCTTGGCTGGACGTAA. P1 and P2 were used for wild type and P1 and P4 for flox genotyping. CRE1 = GCGGTC TGGCAGTAAAAACTATC and CRE2 = GTGAAACAGCATTGCTG TCACTT were used for genotyping Cre recombinase. The PCR was carried out using a thermocycler (PTC-200 MJ Research).

2.2. Echocardiography and electrophysiological studies

Mice were anesthetized with isoflurane (0.8%) and the fur from the mid-neckline to the mid-chest level was removed using a hair remover (Nair). Transthoracic echocardiography was carried out on both *SOD2fl* and *SOD2Δ* mice using a 30 MHz probe with Vevo 3100 Ultrasonograph (VisualSonics). The echocardiography procedures were performed in mice while maintaining heart rate, respiratory rate, and body temperature within standard limits. Ventricular dimensions were measured on M-mode images. The formula [(LVID; d - LVID; s) ÷ LVID; d] x 100 was used to calculate percent fractional shortening (%FS). Electrophysiological studies were performed in mice, as previously described [13]. Four-month-old *SOD2fl* and *SOD2Δ* mice were used for the study. After mice were anesthetized using isoflurane, a catheter inserted through the right jugular vein was advanced down to the right atrium and ventricle. Data were analyzed and obtained with computer-based software (PowerLab 16/30; ADI Instruments).

2.3. RNA isolation and quantitative PCR

The RNeasy mini kit (Qiagen, Chatsworth, CA) procedure was followed according to the manufacturer's instructions to isolate total RNA from mouse hearts. A High-Capacity cDNA Reverse Transcription kit (4368814, Applied Biosystems, Foster City, CA) was used for the cDNA preparation. Taqman fast advanced master mix (4444556, Applied Biosystems, Foster City, CA) was used for the mRNA master mix preparation, and the mRNA levels were measured using the ViiA7 system (Applied Biosystems). Quant Studio™ Real-Time PCR Software v1.3 was used to analyze the threshold cycles (CT) and the amplification of mRNA. The fold-change in expression was calculated using the 2-ΔΔCT method with 18 S RNA as the endogenous control [13].

2.4. Neonatal cardiomyocyte isolation and mitochondrial bioenergetics

Neonatal cardiomyocyte isolation was performed according to the protocol given by Ehler et al. [14]. Briefly, 1- to 2-day-old pup hearts were isolated under sterile conditions. Ventricular tissue was minced and then digested using media containing collagenase. Other cells, such as fibroblast and endothelial cells, were separated from the cardiomyocytes by centrifuging at 300 RPM for 5 min and pre-plating the cells. The neonatal cardiomyocytes obtained were plated in gelatin-coated Seahorse XF microplates for OCR (oxygen consumption rate) and ECAR (extracellular acidification rate) measurement. The mitochondrial isolation was performed according to the method described in Chandra et al. [13], where different batches of mitochondria or cells came from the same littermates. A Seahorse Extracellular Flux (XF-24) analyzer (Seahorse Bioscience, Chicopee, MA) was used to analyze the OCR and ECAR from isolated mitochondria and neonatal cardiomyocytes, as previously described [13]. Briefly, the OCR was measured following sequential addition of oligomycin (1 μg/mL), FCCP (0.5 μM), and rotenone + antimycin A (1 μM). ECAR was conducted in media lacking glucose with the sequential addition of glucose (25 mM), oligomycin (1 μg/mL), and 2-deoxyglucose (25 mM). Both OCR and ECAR values were normalized to the total protein content from the corresponding wells and expressed in pmol/min/μg protein and mpH/min/μg protein, respectively.

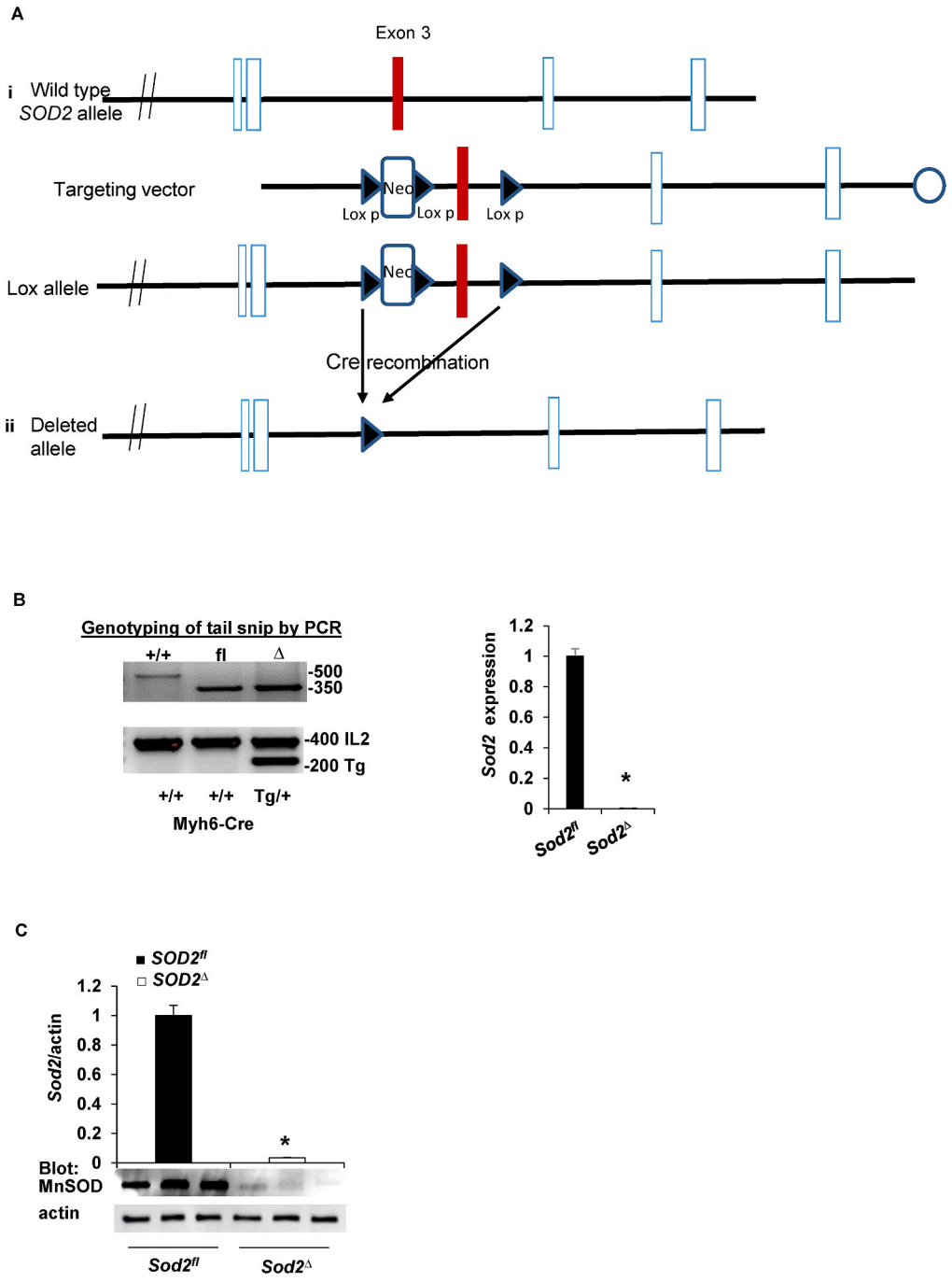

Fig. 1. Generation, genotyping, and confirmation of *SOD2*$^{\Delta}$ mice. A, strategy for generating cardiac-specific alpha myosin-heavy chain *SOD2* knockout mice. i) The *SOD2* genomic structure containing exon 3 (upper) was replaced by a targeting Neo cassette in the expected homologous recombination (lox allele) (lower). ii) After complete Cre-mediated recombination (*SOD2Δ*), the Neo cassette and exon 3 were excised from the genome. B, PCR of DNA (left) obtained from mouse tail snips was screened for the totally recombined allele; orphan *loxP*, 350 bp (fl), and the Cre allele, 200 bp. *SOD2* mRNA expression (right) was measured in heart tissue from *SOD2*^{fl} and *SOD2*$^{\Delta}$ mice and reported relative to values in *SOD2*^{fl} heart tissue (mean ± SD from n = 5 animals per genotype, *P < 0.001). C, Western blotting of heart lysate demonstrates *SOD2* protein expression in *SOD2*^{fl} and *SOD2Δ* with β-actin used as a loading control. *SOD2* expression was normalized to β-actin staining (n = 3 animals) and presented as mean ± SD in arbitrary units in which the density of *SOD2* in the *SOD2*^{fl} samples was set to 1. *P < 0.05 by *t*-test vs. control. D, Immunofluorescence staining of heart section stained with antibody to SOD2 (red) and Troponin I (green) (upper) from *SOD2*^{fl} mice where the arrow indicates SOD2 in cardiomyocytes. SOD2 and Troponin I immunofluorescence (lower) in *SOD2Δ* heart where the arrow indicates SOD2 in other cells. Nuclei were counterstained with DAPI (blue). Note that SOD2 is not apparent in cardiomyocytes from *SOD2Δ* hearts. The result is representative of three independent experiments. Scale bar = 50 μm. E, Kaplan-Meier analysis of survival probabilities for the *SOD2Δ* (n = 85) versus the *SOD2*^{fl} (n = 91) mice. F, The heart of a 4-month-old *SOD2Δ* mouse is significantly larger than that of a *SOD2*^{fl} mouse (scale in mm). Quantification of LV mass and HW/BW of *SOD2*^{fl} and *SOD2Δ* mice. G, Quantification of electrophysiology studies, atrial fibrillation (AF), atrial effective refractory period (AERP), ventricular tachycardia (VT), and ventricular effective refractory period (VERP) of *SOD2Δ* vs. *SOD2*^{fl} mice heart (n = 6, *P < 0.01). H, RT-PCR shows fold differences in the mRNA of *Nppa* and *Nppb* with the value of *SOD2*^{fl} defined as 1 (mean ± SD, n = 5 each). *P < 0.001 compared to control. (For interpretation of the references to colour in this figure legend, the reader is referred to the Web version of this article.)

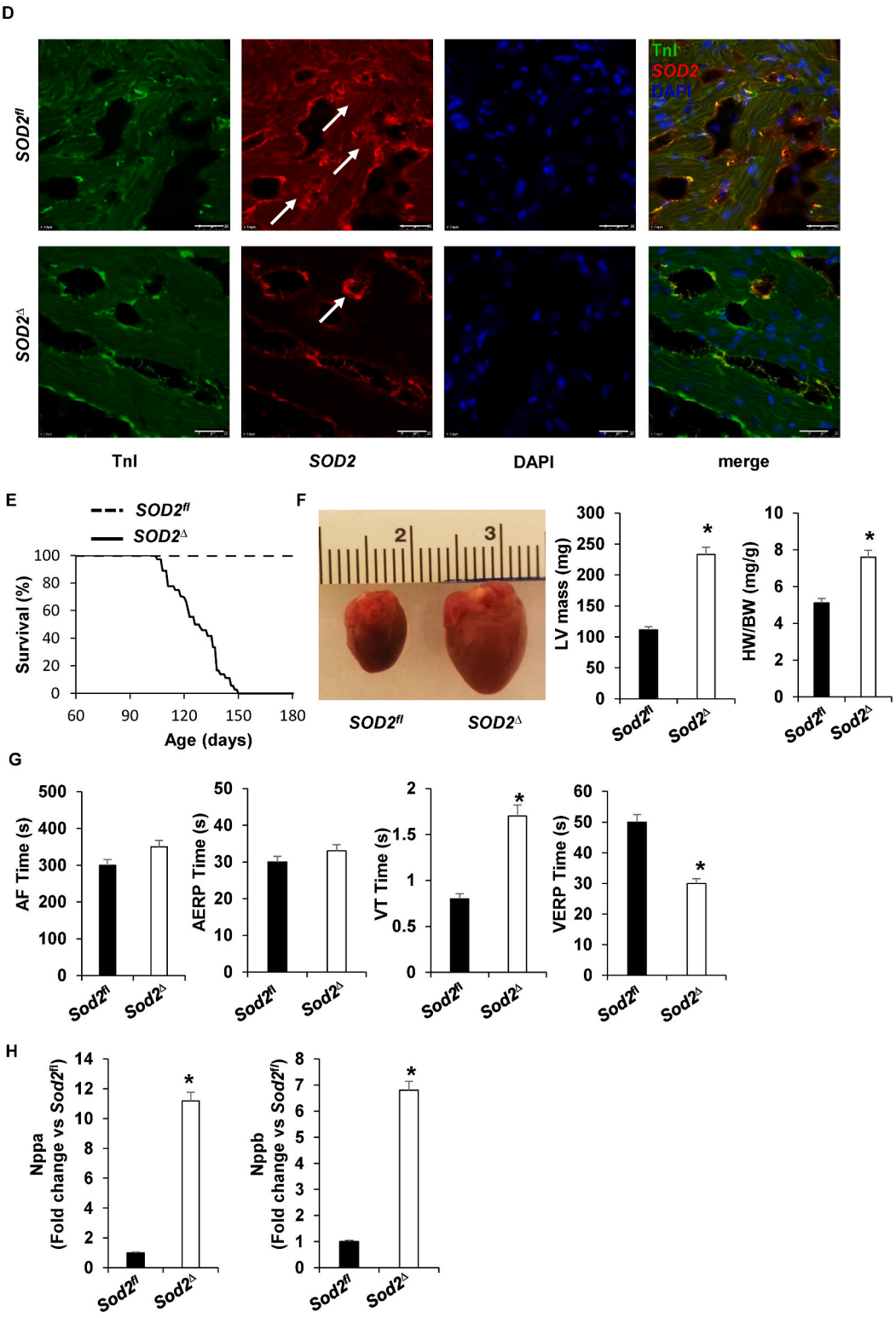

Fig. 1. (*continued*).

2.5. Histology, immunohistochemistry and electron microscopy

For histological analysis, hearts from 4-month-old mice were collected, fixed in formalin, and embedded in paraffin. The mouse hearts were cut in 5-μm sections and stained with Masson's trichrome or Hematoxylin and Eosin. For immunohistochemistry studies, hearts embedded in OCT were sectioned and fixed with ice-cold methanol, followed by permeabilization (0.1% Triton x100) and blocked using 10% goat serum. Images were acquired with a Leica TCS SP5 Confocal microscope and processed using LAS AF SP5 acquisition software. For electron microscopic analysis, left ventricles were collected and fixed with 2% glutaraldehyde (Sigma) followed by 2% PFA in 0.2 M sodium cacodylate (pH 7.4; Sigma) and incubated overnight at 4 °C. Tissues were post-fixed with 1% osmium tetroxide (EM Sciences) in 0.2 M sodium cacodylate (pH 7.4) with a 2 h incubation at 4 °C. A Hitachi transmission electron microscope was used to image the tissue sections.

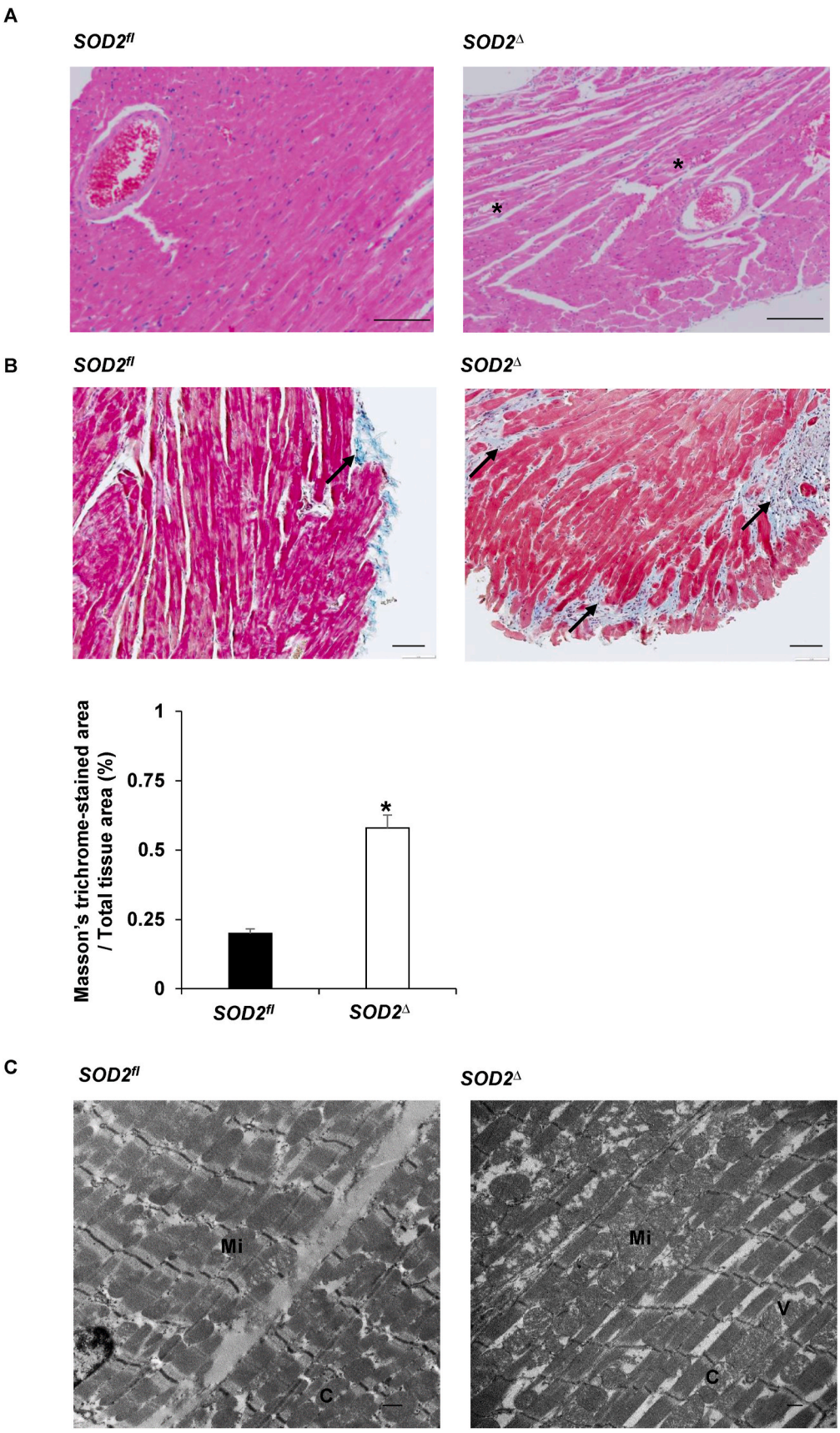

Fig. 2. Cardiac dysfunction was exhibited in *SOD2Δ* mice. A, Representative Hematoxylin and Eosin-stained heart tissue (LV) from *SOD2Δ* as compared to their $SOD2^{fl}$ littermates. Sarcomere disruption is indicated by *. Scale bar = 100 μm. B, Masson's trichrome-staining image (upper) of $SOD2^{fl}$ and *SOD2Δ* heart section (LV). Arrow indicates fibrosis in heart tissue. Scale bars = 100 μm. Quantification of cardiac fibrosis area from Masson's trichrome-stained heart sections (lower). All analyses were carried out in 4-month-old mice. Values are the means ± SD (n = 5). *$P < 0.05$ vs. control group. C, Transmission electron micrograph of 4-month-old

myocardium (LV) from *SOD2Δ* mice as compared to their *SOD2*^{fl} littermates. *SOD2Δ* myocardium showed damaged mitochondria (Mi) with disorganization of cristae (C) and vacuole formation (V) in *SOD2Δ* as compared to *SOD2*^{fl}. Scale bar = 500 nm. D, Quantification of superoxide dismutase (SOD2), CuZnSOD, catalase, and glutathione peroxidase activity (n = 5, *P < 0.001). Assessment of GSH, GSSG, and GSH/GSSG from heart tissue of *SOD2Δ* vs. *SOD2*^{fl} mice. E, Superoxide generation was analyzed using HPLC after staining myocardial tissue with a dihydroethidium fluorescence probe (left). Quantification of mitochondrial superoxide by HPLC after staining with (MitoSOX Red) from mitochondria of heart tissue *SOD2Δ* vs. *SOD2*^{fl} (right). *P < 0.001 compared to control. Mitochondrial homogenate from *SOD2Δ* mice showed significantly increased total HNE adducted protein compared to *SOD2*^{fl}. Left, absolute values of HNE-bound protein levels by slot blot gel analysis. Middle, the normalized % increase of HNE adducted protein in *SOD2Δ* vs. *SOD2*^{fl} (n = 5). *P < 0.001 compared to control. Cardiolipin level of isolated mitochondria from *SOD2Δ* vs. *SOD2*^{fl} mice heart (right) (n = 5). *P < 0.05 compared to control. (For interpretation of the references to colour in this figure legend, the reader is referred to the Web version of this article.)

2.6. Superoxide measurement and activity assays

Superoxide measurement in heart tissues was carried out using high-performance liquid chromatography (HPLC) systems coupled with UV–vis and fluorescence detectors. For mitochondrial superoxide measurements, MitoSOX™ Red (Invitrogen) was used as previously described [13]. *SOD2* activity was assessed using the methods described by Spitz and Oberley (1989) where the Nitro Blue Tetrazolium (NBT)-bathocuproine sulfonate (Sigma) reduction inhibition method was used. Complex I, ATP synthase, DLD, and SDHA activity were measured based upon the procedures of Yan et al. and Zhao et al. [15,16]. 4-HNE bound proteins were detected as previously described [16]. Glutathione measurements were detected as previously described [17]. Cardiolipin was measured from isolated mitochondria from heart tissue using a Cardiolipin Assay Kit (Sigma) according to the protocol provided by the manufacturer.

2.7. Statistical analysis

Unless otherwise stated, data are reported as mean ± standard deviation (SD) for all groups. *In vitro* studies were repeated a minimum of three times. The unpaired Student's *t*-test was used to identify significant differences between groups. Statistical analysis was performed using Graphpad prism 8.0. A P-value of less than 0.05 was considered to be statistically significant.

3. Results

3.1. Generation of cardiac-specific SOD2 knockout mice

Cardiomyocyte-specific *SOD2* knockout mice (*SOD2Δ*) were generated by targeting exon 3 of the *SOD2* locus (Fig. 1A) [11]. *SOD2*^{fl} mice with three *loxP* sites, where two flanking Neo^{r} and a third lox P were inserted at an intron between exon 3 and 4 of the *SOD2* locus, were crossed with mice expressing Cre recombinase under the control of the cardiac-specific alpha-myosin heavy chain promoter (*Myh6-Cre*) [12] to generate conditional *SOD2*-deficient mice (Fig. 1A). Mice were genotyped using DNA extracted from a tail snip of wild type, *SOD2*^{fl}, and *SOD2Δ* mice. The wild-type allele was amplified using primers P1 and P2, producing a 500 bp product; the floxed allele was amplified using primers P1 and P4, producing a 350 bp product. Wild-type mice were identified by a single band at a 500 bp without a Cre band at 200 bp, *SOD2*^{fl} mice had a flox band at a 350 bp without a Cre band at 200 bp, and the *SOD2Δ* mice were differentiated from flox mice by the presence of a Cre band at 200 bp (Fig. 1B). RT-PCR carried out with the cardiac tissue of *SOD2Δ* mice revealed SOD2 mRNA expression to be negligible compared to that in *SOD2*^{fl} mice (Fig. 1B). Immunoblot analysis was performed in the myocardial tissue of *SOD2*^{fl} and *SOD2Δ* mice to confirm *SOD2* protein expression. We detected negligible protein expression of *SOD2* in *SOD2Δ* mice compared to that in *SOD2*^{fl} heart lysates (Fig. 1C), suggesting a sizeable contribution of *SOD2* from cardiomyocytes. Immunohistochemical analysis of heart tissue indicated that SOD2 was not present in cardiomyocytes (Fig. 1D). The remaining *SOD2* expression in the heart of *SOD2*$^{\Delta}$ mice is likely to be from endothelial, fibroblast, or other cells. Thus, the deletion of exon 3 of the *SOD2* gene resulted in the substantial lack of protein in *SOD2Δ*, indicating the successful production of cardiomyocyte-specific *SOD2* knockout mice.

3.2. Mice lacking SOD2 in their cardiomyocytes have shorter life spans and abnormal heart morphology

Unlike global *SOD2* knockout mice, *SOD2Δ* mice were viable and fertile. All mice were able to reach adulthood; however, most of them had a short life span of ~4 months (Fig. 1E). Gross morphological analysis of hearts from these mice showed enlargement, indicating dilated cardiomyopathy (Fig. 1F). The left ventricular (LV) mass and heart weight/body weight (HW/BW) ratio were also significantly elevated in *SOD2Δ* compared to *SOD2*^{fl} control mice (Fig. 1F). Electrophysiological studies done in *SOD2Δ* mice showed shorter ventricular effective refractory periods (VERP) compared to those in their *SOD2*^{fl} littermates. These mice also had a higher incidence of inducible ventricular tachycardia (VT) without any increase in the incidence of atrial fibrillation (AF) or atrial effective refractory periods (AERP) when compared to the controls (Fig. 1G). Natriuretic peptides A and B (*Nppa* and *Nppb*) are secreted by the myocardium in response to cardiomyopathy, so we measured their levels in the failing *SOD2Δ* hearts. As shown in Fig. 1H, an increase in the expression of these cardiomyocyte stress-response genes was observed. Cardiac tissue samples from 4-month-old mice were stained with Hematoxylin and Eosin (Fig. 2A) to compare the myocardium. *SOD2Δ* hearts exhibited sarcomere disarray, whereas *SOD2*^{fl} hearts had no abnormalities (Fig. 2A). Cardiac fibrosis with deposition of connective tissue collagen matrix was assessed by performing Masson's trichome staining. The examination of Masson's trichome-stained heart sections demonstrated fibrosis in the *SOD2Δ* mice (Fig. 2B). Transmission electron microscopy of myocardium showed normal mitochondrial architecture in *SOD2*^{fl} hearts, whereas *SOD2Δ* mitochondria appeared to have vacuole formation with prominent disruption of the cristae and rupture of the double membrane (Fig. 2C). Together, these results suggest that *SOD2* is essential for cardiac function, and its lack leads to dilated cardiomyopathy and heart failure.

3.3. Quenching of ROS blunted due to ablation of SOD2

4-HNE is a highly reactive, toxic aldehyde produced when ROS react with lipids such as cardiolipin, a phospholipid located exclusively in the inner mitochondrial membrane [18–21]. Thus, we investigated whether cardiomyocytes deficient in the mitochondrial-based antioxidant *SOD2* experience an increase in superoxide, promoting the intramitochondrial formation of 4-HNE. *SOD2* activity was drastically reduced in the hearts of *SOD2Δ* mice as compared to those of *SOD2*^{fl} mice, without any alteration in the activity of CuZnSOD, catalase, or glutathione peroxidase (Fig. 2D). We also investigated whether the loss of SOD2 alters GSH and GSSG at the cellular level. GSH, GSSG, and GSH/GSSG ratio in *SOD2Δ* heart tissue did not significantly differ from the *SOD2*^{fl} mice (Fig. 2D). As expected, when superoxide was measured in the tissue and in the isolated mitochondria from *SOD2Δ* hearts, it was found at levels more than 3-fold higher than those in *SOD2fl* mice (Fig. 2E). Mitochondria isolated from *SOD2Δ* hearts displayed an increase in both absolute and percentile 4-HNE adducted protein compared to those of hearts from control mice. The cardiolipin levels were approximately 2-fold lower in the hearts of *SOD2*$^{\Delta}$ mice (Fig. 2E). These results indicate

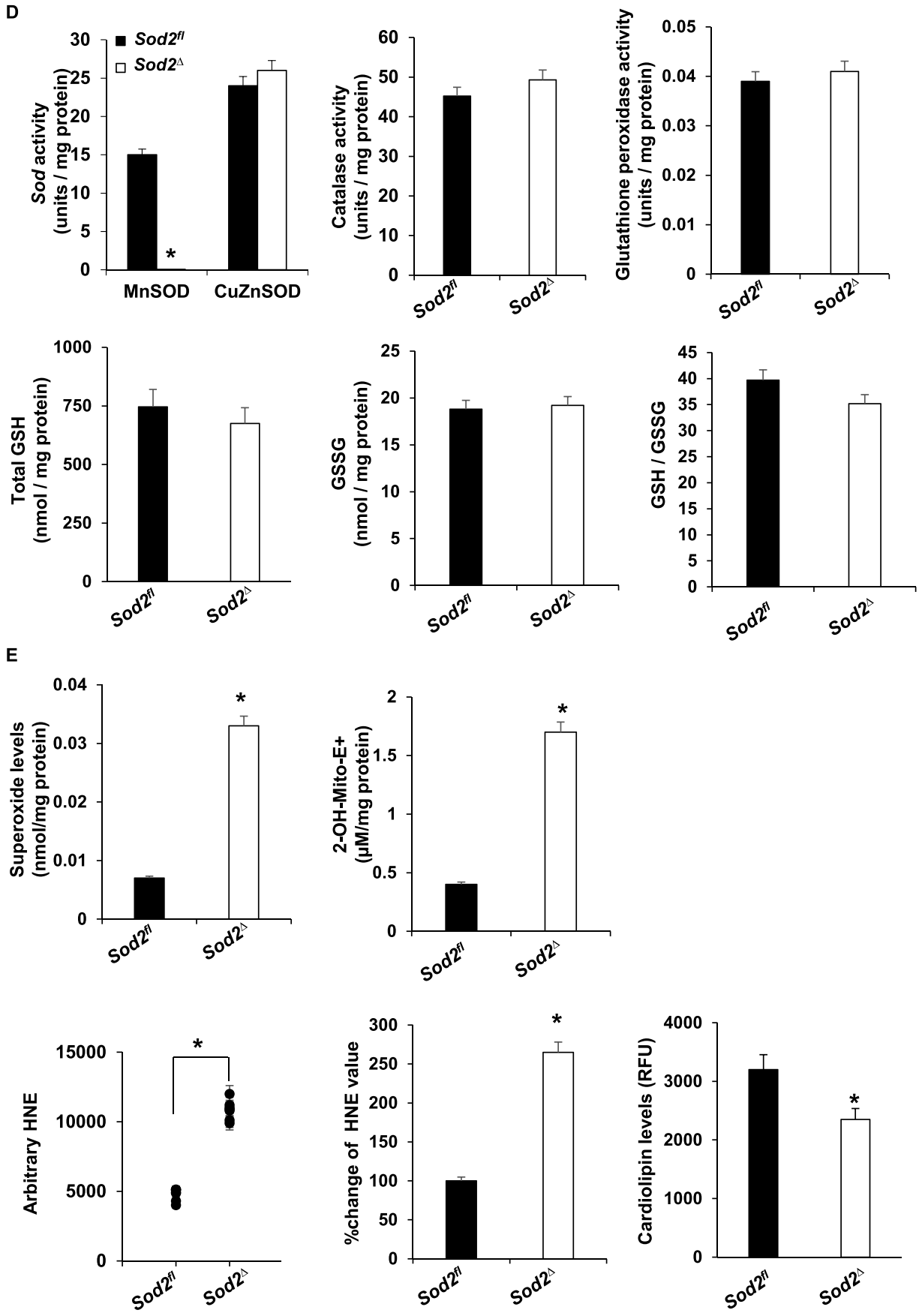

Fig. 2. (*continued*).

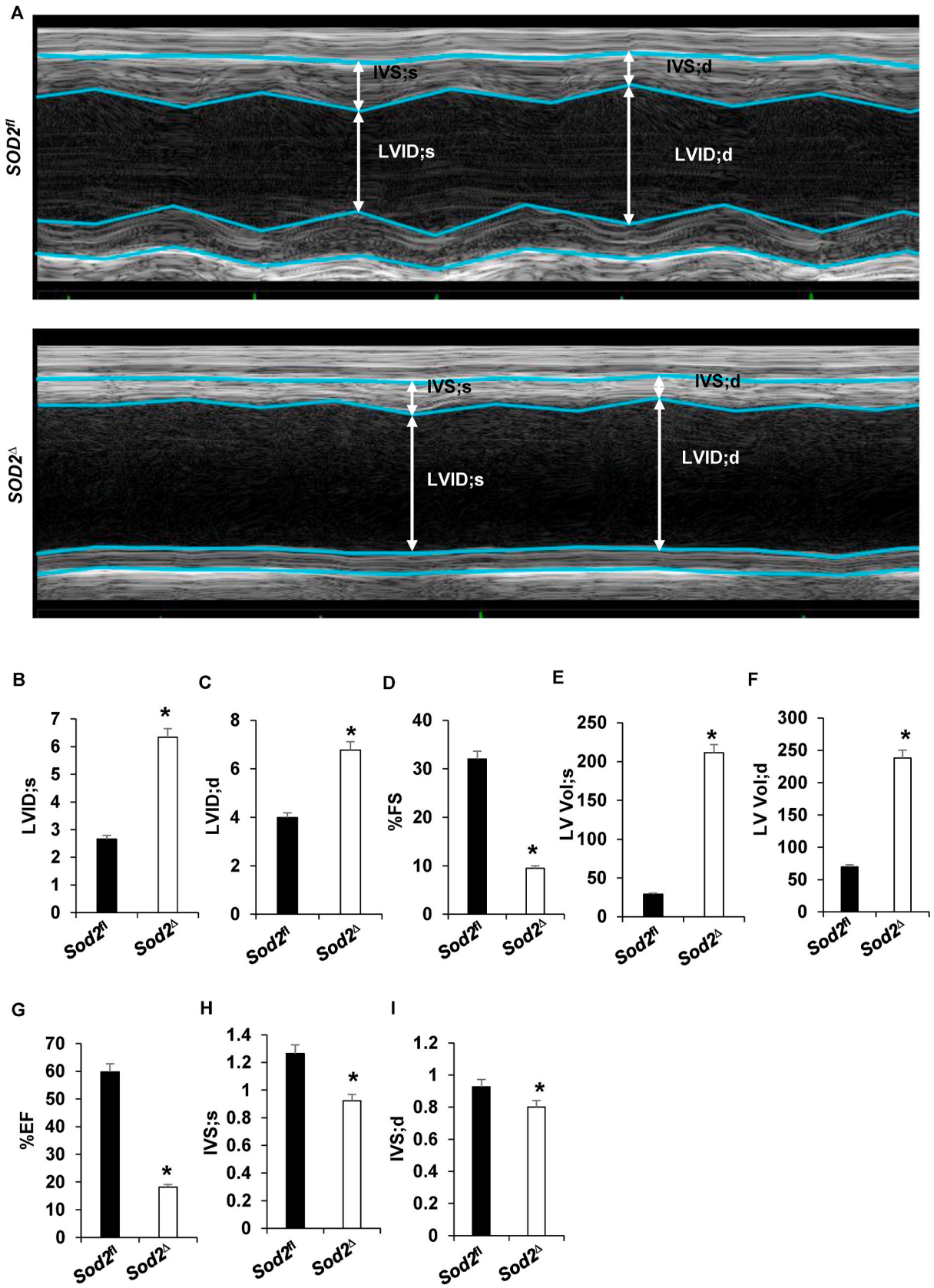

Fig. 3. Echocardiographic indices of contracting *SOD2Δ* mouse hearts (n = 6) (A–I). A, Representative M-mode images of *SOD2*^{fl} and *SOD2Δ* heart. B, systolic left ventricular internal diameter (LVID; s). C, diastolic left ventricular internal diameter (LVID; d). D, percentage fractional shortening (%FS). E, left ventricular systolic volume (LV Vol; s). F, left ventricular diastolic volume (LV Vol; d). G, % ejection fraction. H, systolic intraventricular septum diameter (IVS; s). I, diastolic intraventricular septum diameter (IVS; d).*P < 0.05 compared to control.

that *SOD2* dependent ROS generation leads to the 4-HNE formation in mitochondria.

3.4. Ablation of SOD2 in cardiomyocytes triggers dilation and impairs cardiac function in mice

Prompted by the evidence of mortality and the gross and ultrastructural analysis of heart tissue suggestive of the presence of dilated cardiomyopathy in *SOD2Δ* mice, we performed echocardiography. Echocardiography has been established as an essential tool not only for diagnosis but also for understanding the pathogenesis of dilated cardiomyopathy [22]. Transthoracic M-mode echocardiography of *SOD2Δ* heart tissue (Fig. 3A) demonstrated an increase in left ventricle internal diameter during systole (LVID; s) and diastole (LVID; d) (Fig. 3B–C) accompanied by systolic dysfunction, with a significant reduction in percentage fractional shortening (%FS) and percentage ejection fraction (%EF) (Fig. 3D and G, respectively) compared to measurements in $SOD2^{fl}$ mice. Results also showed increased LV volumes during systole (LV Vol; s) and diastole (LV Vol; d) in *SOD2Δ* mice (Fig. 3E–F). SOD2 deficient mice also showed decreased intraventricular septum diameter during systole (IVS; s) and intraventricular septum diameter during diastole (IVS; d) (Fig. 3H–I). All of the above results confirmed dilated cardiomyopathy in *SOD2Δ* mice.

3.5. Loss of SOD2 in cardiomyocytes shifts energy metabolism from mitochondrial to glycolytic respiration

SOD2 deficiency caused changes in mitochondrial ultrastructure and also led to the formation of toxic aldehyde inside mitochondria; therefore, we sought to identify its effect on energy metabolism and used a Seahorse XF-24 analyzer to measure oxygen consumption and the extracellular acidification rate. For this, we isolated mitochondria from the myocardium of ~4-month-old *SOD2Δ* and SOD2*fl* mice. The quality of mitochondrial isolation was excellent in both the mice strains as indicated by no changes in the activity of fumarase, a mitochondrial enzyme, in the hearts of *SOD2Δ* mice (548 ± 19.6 mU/mg) or their $SOD2^{fl}$ (564 ± 18.7 mU/mg) littermates. Although there was a decrease in OCR during basal conditions and after the addition of the uncoupler FCCP, there was no significant change in OCR after the addition of the complex V inhibitor oligomycin, or the Complex I and III inhibitors Rotenone and Antimycin, respectively (Fig. 4A–B). The resulting data showed a significant reduction in ATP turnover and maximum respiration and spare respiratory capacity in mitochondria of *SOD2Δ* compared to *SOD2*fl heart tissue (Fig. 4C). We isolated neonatal cardiomyocytes from the *SOD2Δ* hearts to measure both OCR and ECAR. OCR measured in neonatal cardiomyocytes showed a pattern similar to that of mitochondria isolated from *SOD2Δ* hearts (Fig. 5A–C). We also measured glycolysis and glycolytic reserve with the Seahorse XF-24 analyzer to determine glycolysis. *SOD2Δ* cardiomyocytes showed a drastic increase in both glycolysis and glycolytic reserve compared to *SOD2fl* cardiomyocytes (Fig. 5D). The compensatory increase in glycolysis could be attributed to impairment in mitochondrial respiration.

3.6. 3.6 Impairment in mitochondrial complex I and V activity in cardiomyocyte-specific SOD2 knockout mice

To gain solid evidence concerning the status of the respiratory complex activity, we extracted mitochondria from both *SOD2Δ* and *SOD2fl* myocardium. Results from the activity assay showed a decrease in the activities of Complex I and Complex V without any change in the activities of SDHA or DLD (Fig. S1).

3.7. The relationship between 4-HNE adducts and mitochondrial respiratory chain complex proteins

The finding that a deficiency in *SOD2* caused an increase in 4-HNE and a reduction in the activity of the mitochondrial complex prompted us to determine whether these mitochondrial complex-forming proteins are potentially responsible for 4-HNE adduction. In the mitochondria of *SOD2Δ* mice, immunoprecipitation of 4-HNE followed by Western blot analysis showed an increase in NDUFS2, SDHA, ATP5B, and DLD. Although Western blot analyses were carried out using both whole heart lysate and mitochondrial lysate, we did not observe any change in protein expression (Fig. 6A; Fig. S2).

4. Discussion

Although the global homozygous knockout of *SOD2* has been shown to cause cardiac pathology [10], it remains unclear whether these defects are caused by combined *SOD2* deficiencies in different cells, or whether a deficiency in cardiomyocytes alone is capable of causing dilated cardiomyopathy. Recently, it has been shown that the homozygous variant in the *SOD2* gene causes fatal dilated cardiomyopathy, but the associated mechanism in the pathogenesis of DCM was not completely investigated [3]. Therefore, for the first time, we generated cardiomyocyte-specific *SOD2Δ* mice using the Cre-lox system (Fig. 1); it is possible that these mice will be used as an important tool to understand lethal dilated cardiomyopathy in humans. In this study, we demonstrated that a loss of *SOD2* in cardiomyocytes leads to cardiac oxidative stress with the generation of intramitochondrial 4-HNE accompanied by adduction with the proteins of the respiratory chain complex and TCA cycle, mitochondrial dysfunction, fibrosis, and a functional impact on the mitochondrial respiratory complex.

Cardiomyocyte-specific SOD2 knockout mice had shorter life spans (Fig. 1E) and died due to complications of dilated cardiomyopathy. *SOD2Δ* heart tissue displayed distinct histological abnormalities, including sarcomere disarray, elevated fibrosis, and abnormal mitochondrial architecture compared to the tissues of *SOD2fl* mice. Transmission electron microscopy was used to visualize vacuole formation along with prominent disruption in the cristae in the mitochondria of knockout mice (Fig. 2). M-mode echocardiography analysis of heart tissue from *SOD2Δ* mice showed a reduction in percentage ejection fraction (%EF) and fractional shortening (%FS) along with increased left ventricular internal diameter (Fig. 3), which is consistent with the characteristic feature of dilated cardiomyopathy seen in other mouse models [23,24]. Levels of the natriuretic peptides *Nppa* (ANF) and *Nppb* (BNP), diagnostic markers for cardiac hypertrophy, and heart failure, were also increased in these mice [25]. Increased incidence of ventricular arrhythmias has been seen in patients with dilated cardiomyopathy [26,27]; therefore, we carried out an electrophysiology study in which mice were subjected to inducible arrhythmia. The results showed an increased occurrence of ventricular tachycardia and a shorter ventricular refractive period in knockout mice (Fig. 1G). It is possible that the ventricular tachycardia observed in our knockout mice could be attributed to ventricular fibrosis [28].

The robust increase in levels of ROS in isolated *SOD2Δ* mitochondria was not compensated by enhancement of the response of other antioxidants such as CuZnSOD, catalase, glutathione peroxidase, or by the levels of glutathione. Only weak levels of compensatory activity in the antioxidant system are observed with SOD2 deficiency, as has been observed previously in the brain, liver, and skeletal muscle-specific SOD2 knockouts [10,29–33]. Instead, it led to a lipid peroxidation reaction, and accumulation of 4-HNE inside the mitochondria (Fig. 2E), which, when assessed using the anti-4HNE antibody, indicated disruption in the redox balance and further damage to the mitochondria. These findings suggest that precise compartmentalization of oxidative stress is sequestrated in mitochondria with minimal leaks to the cytoplasm, which is cleared by cytosol SOD1. When superoxide reacts with the lipid-like cardiolipin, it initiates a cascade generating reactive aldehydes, among which 4-HNE is considered to be both stable and highly toxic, which is why it has been subjected to investigation in various heart-related diseases [34–36]. 4-HNE can modulate signaling by the

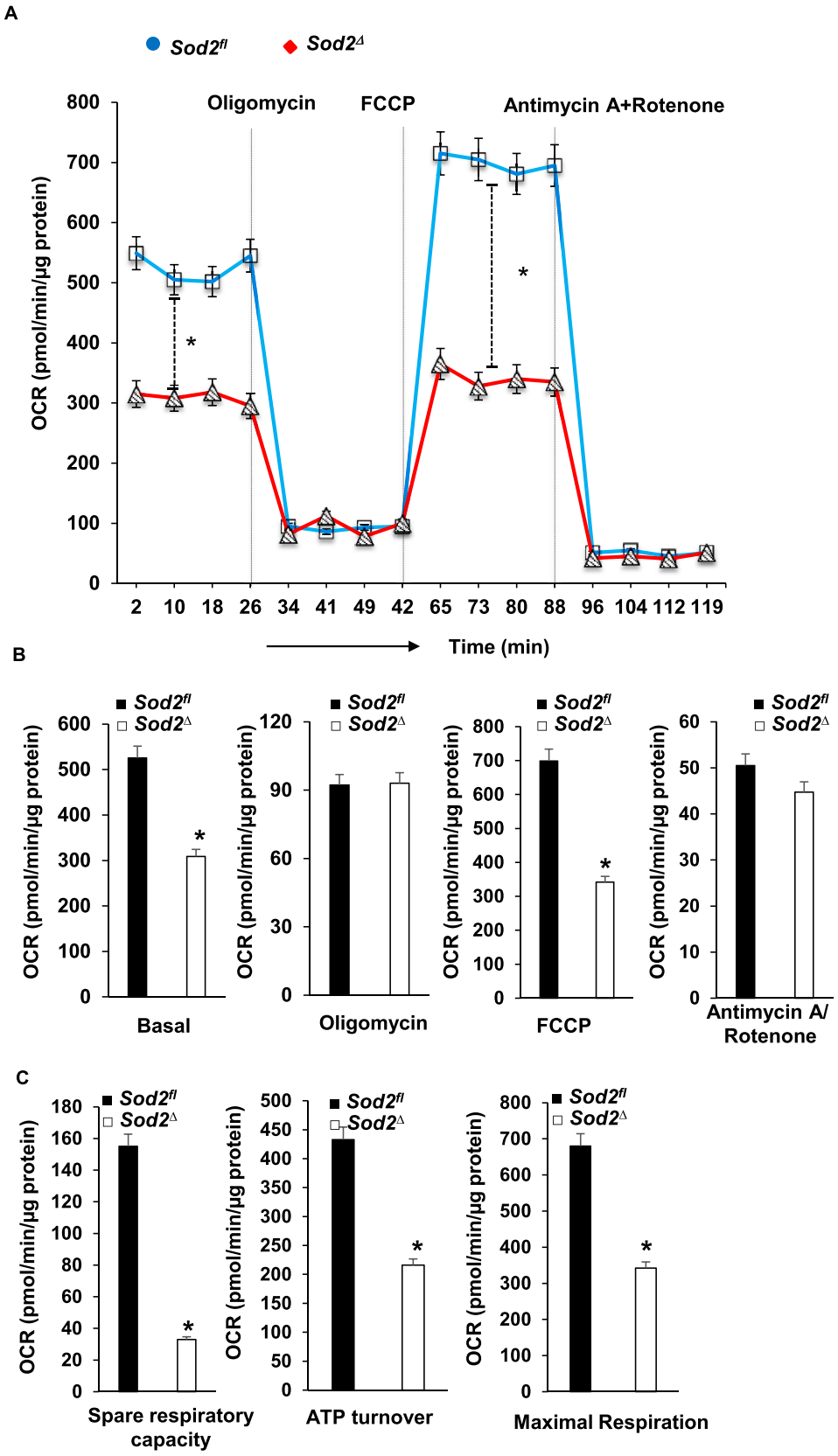

Fig. 4. Mitochondrial bioenergetics in *SOD2Δ* mouse hearts. A and B, the graphs represent oxygen consumption rate (OCR) measurements in isolated mitochondria of *SOD2Δ* vs. $SOD2^{fl}$ hearts at baseline and after sequential addition of oligomycin, FCCP, and Antimycin A + Rotenone. The OCR value is expressed as pmol/min/µg of protein. C, spare respiratory capacity, ATP turnover, and maximum respiration were significantly reduced in *SOD2Δ* mice. All values are mean ± SD (n = 6). *P < 0.001 as compared to control ($SOD2^{fl}$).

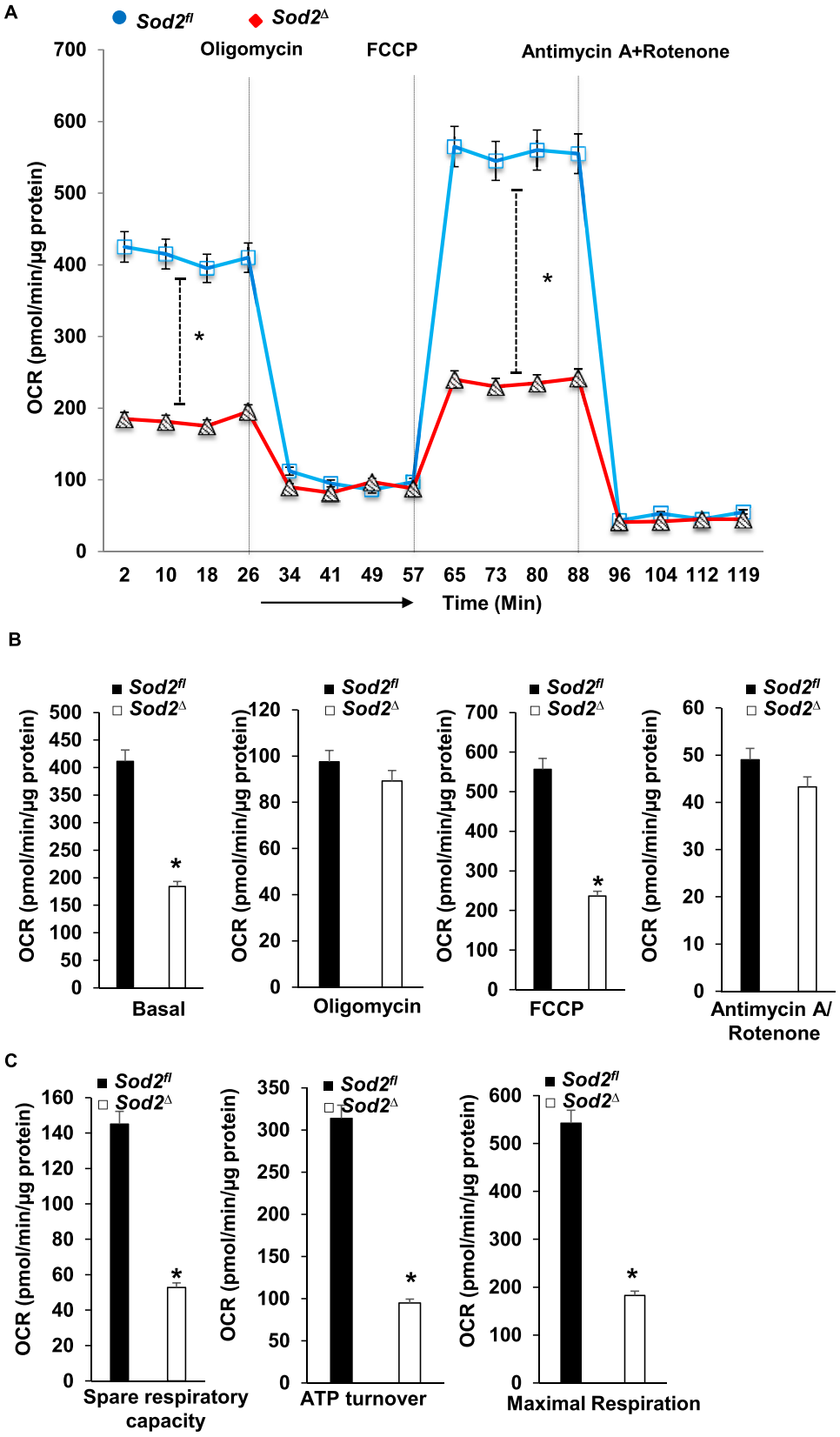

Fig. 5. OCR and ECAR assay in neonatal cardiomyocytes from of *SOD2Δ* and *SOD2*^{fl} mice. A and B, OCR measurement after sequential addition of oligomycin, FCCP, and Antimycin A + Rotenone. C, Mitochondrial respiration, including spare respiratory capacity, ATP turnover, and maximum respiration, were significantly decreased in *SOD2Δ* mice. D, ECAR was measured in neonatal cardiomyocytes over time; the graph represents glycolysis and glycolytic reserve. All values are mean ± SD (n = 5). *P < 0.001 as compared to control (*SOD2*^{fl}).

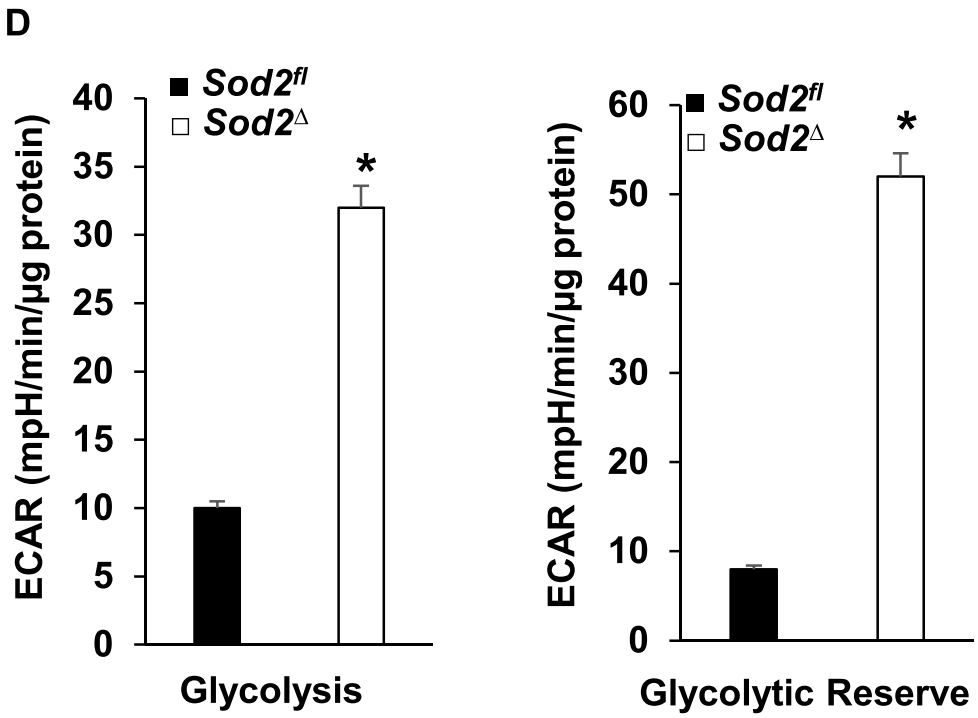

Fig. 5. (*continued*).

adduction of critical cellular components, such as proteins and nucleic acids, and inducing apoptosis of the cell. The amino acids cysteine, lysine, and histidine are targeted by 4-HNE adduction, which could lead to protein inactivation, changes in protein function, and protein cross-linking [37–40]. A decrease in cardiolipin in our knockout mice (Fig. 2E) is consistent, as reported with dilated cardiomyopathy and heart failure [41–43].

Under physiological conditions, oxidative phosphorylation (OXPHOS) contributes 95% of the ATP generation in the heart [44]. The shift in metabolism from OXPHOS to glycolysis observed in the mitochondria and neonatal cardiomyocytes (Figs. 4–5) of our knockout mice support the finding that during certain cardiac pathological conditions [45], a switch in substrate utilization from fatty acid to glucose occurs that mimics the physiological state in neonatal cardiomyocytes. A reduction in the activity of the mitochondrial respiratory complex was observed in human dilated cardiomyopathy and in other mouse models of cardiomyopathy [46–48]. Although we saw a decrease in Complex I and Complex V activities, it was noteworthy that we did not see a decrease in the activity of SDHA, which is part of Complex II and DLD (Fig. S1). This could be due to differences in the amino acid site where 4-HNE modification occurs and proportional to the number of adducts formed [49]. We recently reported that 4-HNE mediated adduction with AIFm2 on His 174 switch protein function, while adduction on Cys 187 did not change [37].

With respect to the previous finding, we wanted to further explore the role of 4-HNE and its effect on different protein subunits of the respiratory complex and TCA cycle. Therefore, we conducted Western blot analysis of proteins after immunoprecipitation reaction with the 4-HNE antibody. NDUFS2, the third-largest, highly conserved subunit of Complex I, is encoded by a nuclear gene; mutation in this gene has been linked to cardiomyopathy, encephalomyopathy, and Leigh Syndrome [50–52]. Complex II, also known as succinate dehydrogenase, is a heterotetrameric protein consisting of four subunits: SDHA, SDHB, SDHC, and SDHD. It performs a dual function: it oxidizes succinate to fumarate in the Kreb's cycle and reduces ubiquinone to ubiquinol, thereby transferring electrons in the electron transport chain [53]. In a mass spectrometric study to find 4-HNE proteins carried out in different cardiac oxidative stress models, such as doxorubicin injection, overexpression of MAO-A oxidase revealed that overexpression of several mitochondrial proteins is involved in functions such as mitoCa2+ transport and mitochondrial bioenergetics. Consistent with the results from these studies, which demonstrated that the respiratory complex proteins NDUFS2 and SDHA are targets of 4-HNE [16,54], we found that both proteins were also modified by 4-HNE in our *SOD2Δ* mice with dilated cardiomyopathy.

ATP synthase, the fifth complex of the respiratory chain is responsible for generating ATP from ADP, and inorganic phosphate is composed of F1 catalytic domain and F0 membrane-bound domain connected by central and peripheral stalk [55]. Subunit ATP5B was found to be adducted by 4-HNE after treatment with doxorubicin in cardiomyocytes [16]. A decrease in Complex V activity in our knockout mice could be attributed to the adduction of ATP5B by 4-HNE, which is one of the subunits of the catalytic F1 domain.

Dihydrolipoamide dehydrogenase (DLD) is a component of 3 multienzyme complexes: pyruvate dehydrogenase complex (PDC), α-ketoglutarate dehydrogenase complex (KDC), and branched-chain α-ketoacid dehydrogenase complex (BCKDC) [56]. Based on the finding that 4-HNE targets DLD [57], we first performed immunoprecipitation reactions using an anti-4-HNE antibody followed by Western blot analysis to show 4-HNE adduction to DLD. This demonstrated that 4-HNE also interferes with an enzyme involved in the TCA cycle in our knockout mice.

Taken together, the results from our study demonstrate that a deficiency of *SOD2* in cardiomyocytes alone is capable of causing mitochondrial dysfunction and subsequent death due to heart failure. Also, *SOD2* dependent ROS generation triggers 4-HNE formation inside mitochondria, which causes modification of the proteins involved in oxidative phosphorylation and the TCA cycle. Our findings suggest that the SOD2 mediated 4-HNE signaling nexus could play an important role in cardiomyopathy. Therefore, therapy for heart failure should target decreasing the aldehyde overload, thereby protecting mitochondrial bioenergetics.

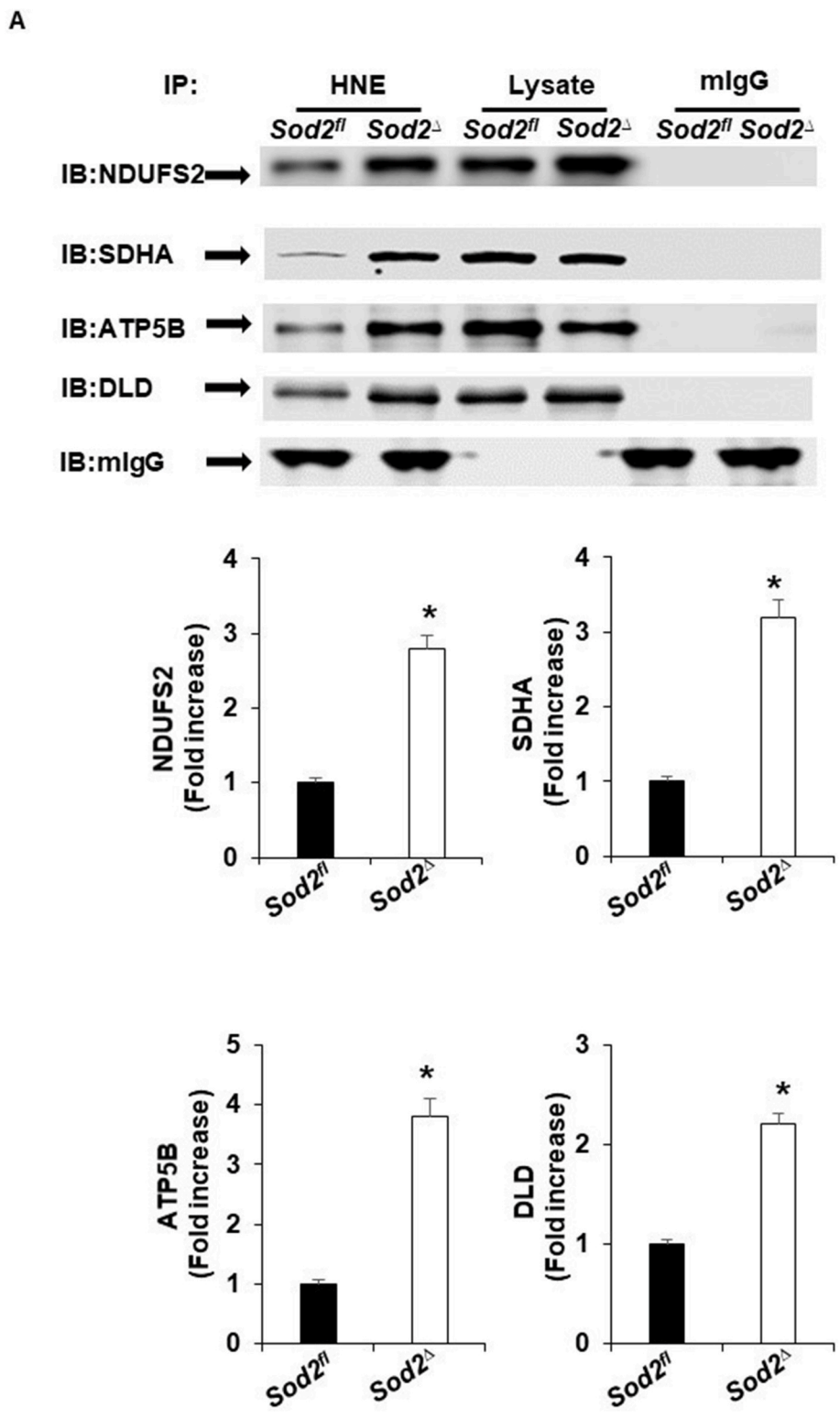

Fig. 6. Representative immunoblots showing the interaction of 4HNE with the proteins of the respiratory complex and TCA cycle. A, murine heart homogenates from *SOD2^{fl}* and *SOD2Δ* mice were immunoprecipitated with mouse 4-HNE antibody (lanes 1 & 2) or mouse IgG antibody (lanes 5 & 6) as a control. Total heart homogenates (20 μg) from IP samples were loaded in lanes 3 and 4. The immunoprecipitates were immunoblotted (IB) with antibodies specific for the indicated proteins (upper). Quantification of immunoprecipitate with mouse 4-HNE antibody (lower). All values are mean ± SD (n = 4). *P < 0.001 as compared to control (*SOD2^{fl}*).

Declaration of competing interest

None declared.

Acknowledgments

The authors thank the Center for Cardiovascular Disease and Sciences (CCDS) imaging and Core for echocardiography and the Animal Care Committee and the Veterinary staff at the Louisiana State University Health Sciences Center-Shreveport for their help with animal experiments at the vivarium. Ronald Maloney provided excellent technical support.

Appendix A. Supplementary data

Supplementary data to this article can be found online at https://doi.org/10.1016/j.redox.2020.101740.

Funding

This work was supported by Louisiana State University Health Sciences-Shreveport Intramural Grant 110101074A to SM; National Institutes of Health grants HL141998 and HL141998-01S1 to SM, AA025744, AA026708, and AA025744-02S1 to MP, AA023610 to HS, HL122354 and HL145753 to MSB, and P20GM121307 to CGK. Funding to pay the publication charges for this article was provided by Dr. Miriyala.

Disclosures

None.

References

[1] P. Elliott, et al., Classification of the cardiomyopathies: a position statement from the European society of cardiology working group on myocardial and pericardial diseases, Eur. Heart J. 29 (2) (2008) 270–276.
[2] E.M. McNally, L. Mestroni, Dilated cardiomyopathy: genetic determinants and mechanisms, Circ. Res. 121 (7) (2017) 731–748.
[3] R. Almomani, et al., Homozygous damaging SOD2 variant causes lethal neonatal dilated cardiomyopathy, J. Med. Genet. 57 (1) (2020) 23–30.
[4] L.D. Osellame, T.S. Blacker, M.R. Duchen, Cellular and molecular mechanisms of mitochondrial function, Best Pract. Res. Clin. Endocrinol. Metabol. 26 (6) (2012) 711–723.
[5] R.Z. Zhao, et al., Mitochondrial electron transport chain, ROS generation and uncoupling (Review), Int. J. Mol. Med. 44 (1) (2019) 3–15.
[6] D.A. Brown, et al., Mitochondrial function as a therapeutic target in heart failure, Nat. Rev. Cardiol. 14 (4) (2017) 238–250.
[7] W. Liu, et al., Formation of 4-hydroxynonenal from cardiolipin oxidation: intramolecular peroxyl radical addition and decomposition, Free Radic. Biol. Med. 50 (1) (2011) 166–178.
[8] E.E. Dubinina, V.A. Dadali, Role of 4-hydroxy-trans-2-nonenal in cell functions, Biochemistry (Mosc.) 75 (9) (2010) 1069–1087.
[9] T. Fukai, M. Ushio-Fukai, Superoxide dismutases: role in redox signaling, vascular function, and diseases, Antioxidants Redox Signal. 15 (6) (2011) 1583–1606.
[10] Y. Li, et al., Dilated cardiomyopathy and neonatal lethality in mutant mice lacking manganese superoxide dismutase, Nat. Genet. 11 (4) (1995) 376–381.
[11] T. Ikegami, et al., Model mice for tissue-specific deletion of the manganese superoxide dismutase (MnSOD) gene, Biochem. Biophys. Res. Commun. 296 (3) (2002) 729–736.
[12] R. Agah, et al., Gene recombination in postmitotic cells. Targeted expression of Cre recombinase provokes cardiac-restricted, site-specific rearrangement in adult ventricular muscle in vivo, J. Clin. Invest. 100 (1) (1997) 169–179.
[13] M. Chandra, et al., Cardiac-specific inactivation of LPP3 in mice leads to myocardial dysfunction and heart failure, Redox Biol 14 (2018) 261–271.
[14] E. Ehler, T. Moore-Morris, S. Lange, Isolation and culture of neonatal mouse cardiomyocytes, JoVE 79 (2013).
[15] L.J. Yan, et al., Reversible inactivation of dihydrolipoamide dehydrogenase by mitochondrial hydrogen peroxide, Free Radic. Res. 47 (2) (2013) 123–133.
[16] Y. Zhao, et al., Redox proteomic identification of HNE-bound mitochondrial proteins in cardiac tissues reveals a systemic effect on energy metabolism after doxorubicin treatment, Free Radic. Biol. Med. 72 (2014) 55–65.
[17] N.S. Rajasekaran, et al., Human alpha B-crystallin mutation causes oxido-reductive stress and protein aggregation cardiomyopathy in mice, Cell 130 (3) (2007) 427–439.
[18] V.R. Mali, S.S. Palaniyandi, Regulation and therapeutic strategies of 4-hydroxy-2-nonenal metabolism in heart disease, Free Radic. Res. 48 (3) (2014) 251–263.
[19] G. Paradies, et al., Oxidative stress, cardiolipin and mitochondrial dysfunction in nonalcoholic fatty liver disease, World J. Gastroenterol. 20 (39) (2014) 14205–14218.
[20] M. Xiao, et al., Pathophysiology of mitochondrial lipid oxidation: role of 4-hydroxynonenal (4-HNE) and other bioactive lipids in mitochondria, Free Radic. Biol. Med. 111 (2017) 316–327.
[21] G. Paradies, et al., Role of cardiolipin in mitochondrial function and dynamics in Health and disease: molecular and pharmacological aspects, Cells 8 (7) (2019).
[22] D.E. Thomas, et al., The role of echocardiography in guiding management in dilated cardiomyopathy, Eur. J. Echocardiogr. 10 (8) (2009) 15–21.
[23] T.L.t. Lynch, et al., Oxidative stress in dilated cardiomyopathy caused by MYBPC3 mutation, Oxid Med Cell Longev 2015 (2015) 424751.
[24] B.K. McConnell, et al., Dilated cardiomyopathy in homozygous myosin-binding protein-C mutant mice, J. Clin. Invest. 104 (12) (1999) 1771.
[25] I.A. Sergeeva, et al., A transgenic mouse model for the simultaneous monitoring of ANF and BNP gene activity during heart development and disease, Cardiovasc. Res. 101 (1) (2014) 78–86.
[26] M.J. Huang Sks, P. Denes, Significance of ventricular tachycardia in idiopathic dilated cardiomyopathy: observation in 35 patients, Am. J. Cardiol. 51 (1982) 507–512.
[27] T. Meinertz, et al., Significance of ventricular arrhythmias in idiopathic dilated cardiomyopathy, Am. J. Cardiol. 53 (7) (1984) 902–907.
[28] H.S. Karagueuzian, Targeting cardiac fibrosis: a new frontier in antiarrhythmic therapy? Am J Cardiovasc Dis 1 (2) (2011) 101–109.
[29] H. Van Remmen, et al., Knockout mice heterozygous for Sod2 show alterations in cardiac mitochondrial function and apoptosis, Am. J. Physiol. Heart Circ. Physiol. 281 (3) (2001) H1422–H1432.
[30] P.T. Kang, et al., Overexpressing superoxide dismutase 2 induces a supernormal cardiac function by enhancing redox-dependent mitochondrial function and metabolic dilation, J. Mol. Cell. Cardiol. 88 (2015) 14–28.
[31] N. Izuo, et al., Brain-specific superoxide dismutase 2 deficiency causes perinatal death with spongiform encephalopathy in mice, Oxid Med Cell Longev 2015 (2015) 238914.
[32] H. Kuwahara, et al., Oxidative stress in skeletal muscle causes severe disturbance of exercise activity without muscle atrophy, Free Radic. Biol. Med. 48 (9) (2010) 1252–1262.
[33] A.R. Cyr, et al., Maintenance of mitochondrial genomic integrity in the absence of manganese superoxide dismutase in mouse liver hepatocytes, Redox Biology 1 (1) (2013) 172–177.
[34] I.E. Blasig, et al., 4-Hydroxynonenal, a novel indicator of lipid peroxidation for reperfusion injury of the myocardium, Am. J. Physiol. 269 (1 Pt 2) (1995) H14–H22.
[35] K. Nakamura, et al., Carvedilol decreases elevated oxidative stress in human failing myocardium, Circulation 105 (24) (2002) 2867–2871.
[36] S. Mak, et al., Unsaturated aldehydes including 4-OH-nonenal are elevated in patients with congestive heart failure, J. Card. Fail. 6 (2) (2000) 108–114.
[37] S. Miriyala, et al., Novel role of 4-hydroxy-2-nonenal in AIFm2-mediated mitochondrial stress signaling, Free Radic. Biol. Med. 91 (2016) 68–80.
[38] D.L. Vander Jagt, et al., Inactivation of glutathione reductase by 4-hydroxynonenal and other endogenous aldehydes, Biochem. Pharmacol. 53 (8) (1997) 1133–1140.
[39] B.J. Stewart, J.A. Doorn, D.R. Petersen, Residue-specific adduction of tubulin by 4-hydroxynonenal and 4-oxononenal causes cross-linking and inhibits polymerization, Chem. Res. Toxicol. 20 (8) (2007) 1111–1119.
[40] J.A. Doorn, D.R. Petersen, Covalent modification of amino acid nucleophiles by the lipid peroxidation products 4-hydroxy-2-nonenal and 4-oxo-2-nonenal, Chem. Res. Toxicol. 15 (11) (2002) 1445–1450.
[41] G.C. Sparagna, et al., Loss of cardiac tetralinoleoyl cardiolipin in human and experimental heart failure, J. Lipid Res. 48 (7) (2007) 1559–1570.
[42] Y. Huang, et al., Cardiac metabolic pathways affected in the mouse model of barth syndrome, PloS One 10 (6) (2015), e0128561.
[43] N. Ikon, R.O. Ryan, Barth syndrome: connecting cardiolipin to cardiomyopathy, Lipids 52 (2) (2017) 99–108.
[44] B. Zhou, R. Tian, Mitochondrial dysfunction in pathophysiology of heart failure, J. Clin. Invest. 128 (9) (2018) 3716–3726.
[45] T. Nagoshi, et al., Optimization of cardiac metabolism in heart failure, Curr. Pharmaceut. Des. 17 (35) (2011) 3846–3853.
[46] A. Buchwald, et al., Alterations of the mitochondrial respiratory chain in human dilated cardiomyopathy, Eur. Heart J. 11 (6) (1990) 509–516.
[47] D. Jarreta, et al., Mitochondrial function in heart muscle from patients with idiopathic dilated cardiomyopathy, Cardiovasc. Res. 45 (4) (2000) 860–865.
[48] N. Joza, et al., Muscle-specific loss of apoptosis-inducing factor leads to mitochondrial dysfunction, skeletal muscle atrophy, and dilated cardiomyopathy, Mol. Cell Biol. 25 (23) (2005) 10261–10272.
[49] M. Breitzig, et al., *4-Hydroxy-2-nonenal: a critical target in oxidative stress?* American journal of physiology, Cell Physiol. 311 (4) (2016) C537–C543.
[50] J. Loeffen, et al., Mutations in the complex I NDUFS2 gene of patients with cardiomyopathy and encephalomyopathy, Ann. Neurol. 49 (2) (2001) 195–201.
[51] V. Guenebaut, et al., Three-dimensional structure of NADH-dehydrogenase from Neurospora crassa by electron microscopy and conical tilt reconstruction, J. Mol. Biol. 265 (4) (1997) 409–418.
[52] L.H. Ngu, et al., A catalytic defect in mitochondrial respiratory chain complex I due to a mutation in NDUFS2 in a patient with Leigh syndrome, Biochim. Biophys. Acta (BBA) - Mol. Basis Dis. 1822 (2) (2012) 168–175.
[53] T.M. Iverson, E. Maklashina, G. Cecchini, Structural basis for malfunction in complex II, J. Biol. Chem. 287 (42) (2012) 35430–35438.
[54] Y. Santin, et al., Mitochondrial 4-HNE derived from MAO-A promotes mitoCa(2+) overload in chronic postischemic cardiac remodeling, Cell Death Differ. 27 (6) (2020) 1907–1923.
[55] A. Dautant, et al., ATP synthase diseases of mitochondrial genetic origin, Front. Physiol. 9 (2018) 329.
[56] R.A. Vaubel, P. Rustin, G. Isaya, Mutations in the dimer interface of dihydrolipoamide dehydrogenase promote site-specific oxidative damages in yeast and human cells, J. Biol. Chem. 286 (46) (2011) 40232–40245.
[57] S.N.A. Hussain, et al., Modifications of proteins by 4-hydroxy-2-nonenal in the ventilatory muscles of rats, Am. J. Physiol. Lung Cell Mol. Physiol. 290 (5) (2006) L996–L1003.